Greenhouse gas policy influences climate via direct effects of land-use change

Andrew D. Jones[1,2], William D. Collins[1,2], James Edmonds[3], Margaret S. Torn[1,2]

Anthony Janetos[3], Katherine V. Calvin[3], Allison Thomson[3], Louise P. Chini[4], Jiafu Mao[5],

Xiaoying Shi[5], Peter Thornton[5], George C. Hurtt[4], and Marshall Wise[3]

Affiliations: 1) Lawrence Berkeley National Laboratory, 2) University of California, Berkeley, 3) Pacific Northwest National Laboratory, 4) Oak Ridge National Laboratory, 5) University of Maryland

Corresponding Author:

Andrew D. Jones

Lawrence Berkeley National Laboratory

One Cyclotron Rd

MS 50A-4037

Berkeley, CA 94720

adjones@lbl.gov

November 9, 2012

Abstract

Proposed climate mitigation measures do not account for direct biophysical climate impacts of land-use change (LUC), nor do the stabilization targets modeled for the 5th Climate Model Intercomparison Project (CMIP5) Representative Concentration Pathways (RCPs). To examine the significance of such effects on global and regional patterns of climate change, a baseline and alternative scenario of future anthropogenic activity are simulated within the Integrated Earth System Model, which couples the Global Change Assessment Model, Global Land-use Model, and Community Earth System Model. The alternative scenario has high biofuel utilization and approximately 50% less global forest cover compared to the baseline, standard RCP4.5 scenario. Both scenarios stabilize radiative forcing from atmospheric constituents at 4.5 W/m^2 by 2100. Thus, differences between their climate predictions quantify the biophysical effects of LUC. Offline radiative transfer and land model simulations are also utilized to identify forcing and feedback mechanisms driving the coupled response. Boreal deforestation is found to strongly influence climate due to increased albedo coupled with a regional-scale water vapor feedback. Globally, the alternative scenario yields a 21st century warming trend that is 0.5 °C cooler than baseline, driven by a 1 W/m^2 mean decrease in radiative forcing that is distributed unevenly around the globe. Some regions are cooler in the alternative scenario than in 2005. These results demonstrate that neither climate change nor actual radiative forcing are uniquely related to atmospheric forcing targets such as those found in the RCP's, but rather depend on particulars of the socioeconomic pathways followed to meet each target.

1 Introduction

Land-use changes exert multiple influences on climate through direct biophysical effects on surface energy and water budgets as well as through changes in net greenhouse gas fluxes (Bonan, 2008; Foley, DeFries, Asner, & Barford, 2005). Climate change mitigation activities to date, however, have focused almost exclusively on the greenhouse gas consequences of land-use change (Marland et al., 2003). None of the proposed regulations or programs, including the UN Reduced Emissions from Deforestation and Degradation (REDD) program (FAO, UNDP, UNEP, 2008), emerging private forest carbon offset programs, agricultural offsets in proposed U.S. climate regulations (U.S. Congress, 2012), or inventories of biofuel-induced land-use change in renewable (USEPA, 2010) and low-carbon (California Air Resources Board, 2009) fuel policies, attempt to account for biophysical effects of land-use change.

This differentiation in how climate effects of land-use change are treated is also evident in the largest global effort to simulate potential changes in future climate, the Climate Model Intercomparison Project, now in its 5th incarnation (CMIP5). CMIP5 utilizes a set of scenarios, or Representative Concentration Pathways (RCPs), generated by integrated assessment models (IAMs) as input to climate models. The RCPs were designed to span a large range of possible radiative forcing in the 21st century with a series of hypothetical global strategies for climate-change mitigation that constrain the future combined radiative forcing from greenhouse gases (GHGs) and aerosols (Moss et al., 2010; van Vuuren et al., 2011).

While the RCP targets include greenhouse gas emissions from land use activities, they do

not incorporate the direct radiative forcings, e.g., changes in albedo, or non-radiative climatic effects, e.g., changes in latent heat flux, that result from those same activities. Nevertheless, these scenarios can be used to investigate the magnitude of the non-GHG forcing, because mapped information on land-use change, derived via the "land-use harmonization" project (Hurtt et al., 2011), is now passed to the Earth system models (Taylor, Stouffer, & Meehl, 2011) and influences their simulations of climate change, much as would be the case if real policies were implemented that did not account for biophysical forcing due to land-use change.

Each of the RCPs was generated with a different IAM, each with its own model-specific assumptions about the technologies, policies, and demographics of the future. Due to this diversity in the underlying IAMs, the global patterns of deforestation and afforestation present in the various RCP scenarios are essentially uncorrelated with the atmospheric forcing target levels (van Vuuren et al., 2011), potentially introducing unsystematic variation in global and regional patterns of climate change across the RCP's. That is, RCP2.6 (a scenario that reaches a global radiative forcing target of 2.6 W/m^2) shows widespread deforestation over the 21st century, whereas RCP4.5 shows widespread afforestation and RCP6.0 and RCP8.5 each show a mix of deforestation and afforestation in different regions (P. J. Lawrence et al., 2012b).

The decoupling of greenhouse gas targets and land-use change within integrated assessment models is highlighted by Wise et al. (2009), who find that equivalent greenhouse gas targets can be reached with dramatically different patterns of land use depending on what kind of tax is used to achieve the target. The present study examines in detail a similar set of

scenarios generated within the newly coupled integrated assessment and Earth system model known as the Integrated Earth System Model (iESM) (Edmonds et al., submitted). We compare the standard CMIP5 RCP4.5 scenario and an alternative RCP 4.5 replication in which the forcing target is achieved through a tax on fossil fuel and industrial carbon only, leading to large-scale expansion of crops and loss of forest cover.

Many modeling studies have examined biophysical and/or biogeochemical climate effects of hypothetically removing or replacing whole ecosystems – e.g., complete deforestation or afforestation of a given region (Bala et al., 2007; Betts, 2000; Gedney & Valdes, 2000; McGuffie, Henderson-Sellers, Zhang, Durbidge, & Pitman, 1995; Swann, Fung, Levis, Bonan, & Doney, 2010). These studies tend to produce robust signals and shed light on the role that those ecosystems play in the climate system. Another class of studies examines realistic estimates of past land-use change (Betts, Falloon, & Goldewijk, 2007; Findell, Shevliakova, Milly, & Stouffer, 2007; Kvalevåg, Myhre, Bonan, & Levis, 2009; P. J. Lawrence & Chase, 2010; Pitman et al., 2009), while only a few studies have examined plausible future scenarios of land-use change (Arora & Montenegro, 2011; Feddema et al., 2005). Gaps remain in distinguishing the detailed mechanisms by which land-use change causes observed changes in climate. For instance, none of these studies compared coupled model surface flux responses to offline surface fluxes with fixed atmospheric forcing, although such a comparison could illuminate the role of atmospheric feedback mechanisms.

By examining two scenarios that follow identical atmospheric forcing trajectories from GHG and aerosols, but with different policy prescriptions and thus different patterns of land-

use change, this study uniquely examines the role that policy design can have in influencing climate via the biophysical effects of land-use change. That is, we show that global mean temperature, radiative forcing, and the spatial pattern of climate change can differ greatly as a function of the policy mechanism chosen to meet an atmospheric forcing target, a result that has implications for the CMIP5 "parallel process" (Moss et al., 2010) by which differing socioeconomic scenarios are to be paired with each RCP scenario.

Agricultural expansion in the alternative RCP4.5 scenario is both widespread and intense, but the net result avoids the total removal of whole ecosystems explored by previous studies. Global forest cover in 2100 is reduced by 52% relative to the standard RCP4.5. Thus, this alternative scenario can be thought of as a hypothetical upper bound on agricultural expansion and an example of the importance of policy design details. In addition to fully-coupled climate simulations, we perform a series of offline radiative transfer and offline land model simulations to isolate forcing and feedback mechanisms that contribute to the Earth system response to land-use change. These simulations allow us to compare changes to surface and planetary energy budgets conditioned on the inclusion or exclusion of atmospheric feedback mechanisms. Breaking the climate system response down into component mechanisms provides insight into the drivers of the observed signals and can generate hypotheses regarding the response to different kinds of land-surface change. The use of offline radiative transfer simulations also allows us to compute the radiative forcing associated the modeled pattern of land-use change, a metric that plays an important role in climate policy as it is used to weigh the magnitude of climate perturbation by different forcing agents. While some of the aforementioned studies have computed the radiative

forcing from various patterns of land-use change, e.g., (Betts, 2000), this study is unique in its side-by-side comparison of offline and coupled surface flux responses and so is able to provide new insight into the mechanisms of large-scale land-use change influences on climate.

2 Methods

2.1 Scenarios

The scenarios of anthropogenic activity examined in this study are generated by the Global Change Assessment Model (GCAM) (Kim, Edmonds, Lurz, Smith, & Wise, 2006), one of the four integrated assessment models used to generate scenarios as part of the Coupled Model Intercomparison Project Phase 5 (CMIP5) (Taylor et al., 2011). Each scenario describes future emissions and land use activities for the period of 2005 to 2100. The baseline scenario in this study is the standard CMIP5 Representative Concentration Pathway 4.5 (RCP4.5), in which a universal carbon tax (UCT) is applied in order to stabilize radiative forcing from greenhouse gases and aerosols at 4.5 W/m^2 (Thomson et al., 2011). For the purposes of scenario generation, radiative forcing is calculated within GCAM by the Model for the Assessment of Greenhouse-Gas Induced Climate Change (MAGICC) (Meinshausen, Raper, & Wigley, 2011), version 5.3. Radiative forcing from dynamic changes in surface physical properties – i.e., alterations to the land-surface albedo – is not accounted for within MAGICC, nor are forcing from mineral dust and nitrate. In this scenario, agricultural technology improvements combined with the high price of emitting terrestrial carbon lead to

afforestation worldwide with a corresponding contraction in global crop area. Biofuels play an expanded role in both the energy and land use mix.

In the alternative scenario, the same target of 4.5 W/m^2 is reached via a fossil fuel and industrial carbon tax (FFICT), under which deforestation is not penalized directly for the resultant increases in CO_2 from disturbance of forest soils and reduction in woody carbon storage. However, since the target is based on atmospheric radiative forcing, fossil fuel and industrial sector emissions must therefore be reduced further in the FFICT scenario relative to the UCT scenario in order to compensate for greater land-use change emissions. Thus, while the end-of-century CO_2 concentrations are nearly identical within GCAM between the UCT and FFICT scenarios (526 and 511 ppm respectively), the relative contribution of fossil fuel emissions versus land-use change emissions to the change in concentration is much higher for the UCT scenario (97%) than for the FFICT scenario (44%). Land-use change emissions increase by an order of magnitude in the FFICT scenario, from 28 to 479 PgC.

The expansion of agriculture and decline in fossil fuel emissions in the FFICT scenario is driven largely by bioenergy combustion for electricity and liquid fuel production combined with carbon-capture and storage, which represents a low cost package of technologies for displacing fossil fuel emissions within GCAM in the absence of a direct deforestation penalty. This leads to a positive feedback whereby deforestation for biofuels increases atmospheric CO_2 and induces a need for more biofuels in order to meet the policy target. As biofuel production expands, both biofuels and traditional crops are pushed to ever more

marginal land where greater areas are required to produce the same yields. The net effect of these dynamics is a dramatic expansion of agriculture, replacing roughly 50% of global forest cover by the final decade of the century (see Figure 1). However, it should be noted that the footprint of bioenergy could be smaller if one assumes higher rates of future crop yield improvements than characterize these two scenarios (Thomson et al., 2010).

2.2 Coupling to the Earth system model

The present study is part of a larger effort to create an Integrated Earth System Model (iESM), which aims to couple the economic portions of the GCAM integrated assessment model with the Global Land-use Model (GLM) (Hurtt et al., 2011; 2006) and the Community Earth System Model (CESM) (Bitz et al., 2012; Gent et al., 2011), a physical Earth system model featuring component models for the atmosphere, ocean, land, and sea ice. The eventual goal is to implement a two-way coupling within a single integrated system whereby economic decisions in GCAM translate directly into trace gas fluxes and land-use changes in CESM while changes in climate within CESM feed back onto crop yields, heating and cooling demands, etc. in GCAM.

This study utilizes the one-way iESM coupling procedure with information flowing from GCAM to GLM to CESM. The GLM is needed to downscale land-use change, modeled at the 14 economic region scale in GCAM, to a 0.5 degree latitude-longitude grid. GLM computes estimates of secondary land area, and spatially allocates wood harvest values (in carbon units) to areas of primary and secondary ecosystems. It also "harmonizes" the data to ensure a continuous transition from historical land-use data. These values are then translated into changes to the areas occupied by the plant functional types implemented in

the Community Land Model (CLM) (D. M. Lawrence et al., 2012a), the land model component of CESM, following the procedure developed by P. J. Lawrence et al. (2012b), and upscaled to the 0.9 x 1.25 degree latitude-longitude grid used in CLM. Land-use changes are linearly interpolated between each 15-year GCAM time step in order to provide a dynamic land-use change dataset. Urban area does not change. This entire procedure is consistent with that utilized in the CMIP5. Thus we are able to reproduce the land-use change dataset used by the National Center for Atmospheric Research (NCAR) as input to CESM for the standard RCP4.5 scenario, which we refer to as UCT.

In order to isolate the biophysical climate effect of reaching the same atmospheric forcing target with different patterns of land use, we force CESM with identical concentrations of atmospheric greenhouse gases and aerosols derived from the UCT scenario. Thus, the full prognostic carbon cycle within CESM is not exercised for this experiment. Rather, we rely on GCAM's estimation of the CO_2 emissions associated with both fossil fuel use and land-use change and the resultant impact on atmospheric concentrations. Aerosol concentrations and deposition rates were computed from emissions as part of the CMIP5 process utilizing an offline atmospheric chemical transport model (Lamarque et al., 2011). We adopt this procedure despite differences in the trajectory and mix of greenhouse gas and aerosol forcing agents between the GCAM versions of the UCT and FFICT scenarios. The original FFICT scenario has greater forcing from methane and nitrous oxide due to greater agricultural activity as well as transiently higher levels of forcing from black carbon from biomass burning. The trajectory of forcing differs as well, with the FFICT scenario overshooting then declining to the target value of 4.5 W/m^2 and the UCT scenario gradually

building up to the same target. However, CO_2 concentrations are essentially equal in the two GCAM scenarios. Thus by adopting the UCT concentrations for all atmospheric constituents, we eliminate variation in the behavior of non-CO_2 forcing agents. 95% of the UCT forcing in 2100 and 94% of the FFICT forcing in 2100 comes from well-mixed GHGs. Thus, we expect that differences in forcing trajectory would be more important than differences in the mix of forcing agents.

We run CESM at approximately 1 degree (0.9 x 1.25) resolution in a fully coupled transient mode with a dynamic ocean, Community Atmosphere Model 4 (CAM4) physics (Neale et al., submitted), and an active carbon-nitrogen biogeochemical model within CLM (Thornton, Lamarque, Rosenbloom, & Mahowald, 2007). The full carbon cycle is not active since atmospheric concentrations of greenhouse gases and aerosols are prescribed as discussed above. We use the standard CLM crop plant functional type, which is identical to the C3 grass plant functional type. Initial conditions for the component models are taken from a 20th century NCAR simulation beginning from equilibrium pre-industrial conditions.

We use a version of CESM that differs from the official release version 5 used for the CMIP5 in a handful of ways, most of which do not materially alter the climate simulation. The most notable difference is that the beta version 15 we have adopted corrects the orbital forcing observed by the sea ice model to be consistent with the other model components. Previous versions held the orbital forcing of the sea ice constant. As discussed further below, we compare this simulation of the UCT scenario (standard RCP4.5) to an ensemble of 5 simulations performed at NCAR using CESM release version 5 for CMIP5. Despite

differences between the version that we use and that used for CMIP5, the mean global temperature response and spatial pattern of temperature response as revealed by fingerprinting methods (discussed further below) from our simulation fall within or near the 95% confidence interval around the ensemble mean taken from the 5 CMIP5 runs. Thus we are confident that we can reasonably replicate the standard RCP4.5 scenario using the model version and configuration options chosen.

2.3 Use of CMIP5 Data

As part of CMIP5, researchers at NCAR have made available the outputs of 5 simulations of the RCP4.5 scenario (our UCT scenario), each with varying initial conditions. These were performed at 0.9 x 1.25 degree resolution using identical configurations, but a slightly different model version than the one that we used for UCT and FFICT as discussed above. We analyze these data to derive estimates of model internal variability in order to evaluate whether differences observed between the UCT and FFICT scenarios are statistically significant. We also evaluate whether our UCT scenario is statistically indistinguishable from the standard CMIP5 RCP4.5 scenarios.

In addition, we utilize 3-hourly atmospheric history outputs from one of the CMIP5 RCP4.5 simulations to drive the offline CLM simulations discussed below.

2.4 Fingerprinting Method

We estimate the spatial pattern or “fingerprint” of the warming trend within each simulation using a method based on empirical orthogonal function (EOF) analysis, which has been

employed in the climate change detection and attribution literature, e.g., (Santer et al., 2004). For computational reasons, we first we aggregate the temporally and spatially varying surface temperature data to annual time steps at approximately 8° x 8° resolution. We take the fingerprint to be the first EOF obtained from the anomalies of this aggregated data set. The first EOF describes the dominant mode of variance within the data – in this case the overall warming trend over time.

2.5 Offline Land Model Simulations

To isolate the first-order land surface response to changes in vegetation due to land-use change, we perform an offline land model simulation in which atmospheric conditions are held fixed at the conditions exhibited in the UCT scenario, but the pattern of land-use change is matched to that in the FFICT scenario. Thus the effect of rising GHG concentrations are present in the atmosphere, but the effects of land-use change on water vapor, clouds, radiation etc. are deliberately omitted. We call this the FFICT-offline scenario. The atmosphere is forced with 3 hourly data taken from one of the NCAR RCP4.5 simulations performed for CMIP5. CLM has built-in algorithms for interpolating the 3-hourly atmospheric data to the 30-minute timestep that we use, including an adjustment to the incoming solar radiation that accounts for the cosine of the zenith angle at each timestep. In order to verify that this offline technique adequately reproduces the UCT climate, we also perform an offline UCT scenario (UCT-offline) that forces the atmosphere as above while maintaining the UCT pattern of land-use change. A finding of congruence between the UCT and UCT-offline scenarios indicates that we have successfully reproduced the UCT climate in the offline simulations.

2.6 Offline Radiative Transfer Calculations

To calculate the radiative forcing due to land-use change, we utilize an offline version of the CESM atmospheric model, the Community Atmosphere Model (CAM). This offline version of CAM, known as PORT (Conley, Lamarque, & Vitt, 2012), runs only the radiative transfer calculations and is forced with instantaneous 3-dimensional state information saved from the UCT scenario at a rate of 240 samples per model year. The samples are evenly distributed over seasonal and diurnal timescales. By substituting surface albedos from the FFICT-offline scenario into PORT driven by the UCT atmospheric states, we obtain an estimate of the change in top-of-atmosphere net absorbed solar radiation that is free from atmospheric feedbacks.

3 Results

3.1 Global and Regional Temperature Trends

The simulated globally averaged warming trend over the 21st century differs by 0.5 °C between the UCT and FFICT scenarios, which exhibit warming trends of 1.2 and 0.7 °C per century respectively (Figure 2). These trends are relative to the first decadal mean of each simulation (2005-2014). Considering the ensemble mean and 95% confidence intervals surrounding this mean taken from the five RCP4.5 scenarios run at NCAR for CMIP5 (Figure 2) it is clear that the FFICT scenario lies well outside the range of internal variability exhibited by the model, indicating that the temperature differences are statistically significant. Meanwhile, the fact that the UCT scenario lies mostly within the confidence

interval around the CMIP5 ensemble mean indicates that we have successfully replicated the RCP4.5 scenario at this scale despite minor differences in model version.

Figure 3 shows the spatial pattern of the temperature trends in the two scenarios, calculated by subtracting the mean of the first simulation decade (2005-2014) from the last (2090-2099) for each scenario. The UCT pattern of warming is typical of greenhouse gas-induced climate change with greater temperature change at high latitudes and over land. The FFICT pattern, however, actually shows a cooling trend in some regions, particularly near areas of boreal deforestation in eastern Siberia and portions of Canada. Other regions show no trend or trends that are similar to those found in the UCT scenario.

The differences between the scenarios are more clearly shown in the seasonal June-July-August (JJA) and December-January-February (DJF) temperature differences between the scenarios for the final simulation decade (Figure 4). There is a clear pattern of relative cooling (i.e., less warming) in the FFICT scenario over much of the land area above 50 degrees latitude. This reduction in warming is strongest over the boreal forests and the Barents Sea and extends to the northeast of Finland, particularly during the northern hemisphere winter when the relative cooling is more than 6 °C in some locations. The strongest cooling is found during northern hemisphere spring (not shown), consistent with Bonan et al. (Bonan, Pollard, & Thompson, 1992). There is also a widespread but modest cooling on the order of 1 °C present over much of the Arctic Ocean during northern hemisphere winter and over mid-latitude oceans during northern hemisphere summer.

While smaller in spatial extent, there are also regions of the tropics at the edges of the Amazon and Congo forests where the FFICT scenario exhibits higher temperatures than the UCT scenario. These are on the order of 1 °C.

Stippling in Figure 4 indicates those gridcells for which the FFICT value lies outside of the 95% confidence interval around the NCAR RCP4.5 ensemble mean. We avoid the problem of underestimating variance due to temporal autocorrelation by using the ensemble variance rather than a time-series of values from a single simulation. However, due to spatial autocorrelation and the finiteness of the sample, it is still likely that more than 5% of the gridcells would display significance even if the FFICT scenario were drawn from the same distribution as the RCP4.5 ensemble (Livezey & Chen, 1983). Indeed, 20% of the UCT scenario (identical to RCP4.5 modulo differences in model version) gridcells are found to be significant using this test for the end-of-century decadal mean temperature difference (not shown). However, many more (71%) of the FFICT gridcells are significant (panel A).

3.2 Spatial Fingerprint of the Warming Trend

Fingerprint analysis provides an alternative way to characterize the spatial significance of the pattern of warming present in the FFICT vs. the UCT scenario. The fingerprints of the UCT and FFICT warming trends are shown in Figure 3. Because rising GHG concentrations and land-use change trends are correlated in these scenarios (i.e., they are not orthogonal processes), their combined effect on surface temperature is mixed, at least partly, in the fingerprint obtained from EOF analysis. As might be expected, the fingerprints fairly closely track the decadal temperature difference between the first and last simulation decade

(also shown in Figure 3). The effect of Boreal deforestation in the FFICT fingerprint is evidenced by diminished warming at high latitudes and a patch of cooling over Eastern Siberia.

We can readily show that the differences between the UCT and FFICT fingerprints are statistically significant and probably do not result from internal variability of the models. The demonstration follows by comparing the FFICT fingerprint against the fingerprints obtained from each of the NCAR RCP4.5 ensemble members. The analytical approach treats each fingerprint as a vector in n-dimensional space where n is 864, the number of gridcells present at the resolution chosen for this analysis. We then compute the angle between each fingerprint and the fingerprint obtained from the RCP4.5 ensemble mean in that n-dimensional space. The ensemble members cluster near the ensemble mean at a mean angle of 7.0° with a standard deviation of 1.3°. The FFICT fingerprint, on the other hand, is rotated by 19.5° from the ensemble mean. Since this angle differs from the corresponding angles for the RCP4.5 ensemble by more than 9 standard deviations, the differences between the FFICT and ensemble mean are therefore highly statistically significant. Thus, even if we are agnostic about the functional form of the distribution of angles around the ensemble mean, we can conclude from Chebyshev's inequality that it is very unlikely to obtain the FFICT fingerprint from model internal variability.

3.3 Surface Energy Budget Changes

The FFICT-offline simulation, which holds atmospheric conditions fixed at UCT values, indicates that the first order effect of changing vegetation from the UCT to FFICT scenario

is an increase in reflected solar radiation of 2.2 W/m^2 averaged over the global land surface during the final simulation decade. As shown in Figure 5, this increase in reflected solar radiation is balanced by decreases in sensible (-2.0 W/m^2) and latent (-0.7 W/m^2) heat fluxes, as well as a small increase in emitted longwave radiation (0.5 W/m^2).

Allowing the atmosphere to respond to these changes results in feedback processes that further alter each term of the surface energy balance. In the fully coupled case, altering land use from the UCT to FFICT scenario results in an even larger increase in reflected solar radiation of 4.0 W/m^2. The corresponding changes in sensible (-1.4 W/m^2) and latent (-1.8 W/m^2) heat fluxes are shifted more heavily to decreases in latent heat flux, and there is a large decrease in emitted longwave radiation (-4.1 W/m^2), reflecting the decrease in surface temperature. The increase in reflected solar radiation is partly explained by an increase in surface insolation of -1.7 W/m^2, which appears as a negative term in the energy budget in order to maintain the sign convention that all fluxes are positive upward. Likewise, the large decrease in emitted longwave is offset by an even larger decrease in downward longwave radiation of 4.8 W/m^2, which we show later is related to changes in the greenhouse effect of water vapor. Both the offline and coupled surface energy budgets balance at the 0.05 W/m^2 level. We do not account for changes in ground heat storage and the latent heat of fusion in this analysis.

Figure 6 shows the equivalent regional energy budgets averaged over the boreal and tropical forest areas. We define boreal as all land area from 45 to 65 degrees N and tropical as all land area from 15 degrees S to 10 degrees N. While the general pattern of flux changes is

similar to the global pattern in each region, the scale of change in the boreal zone is much larger despite similar levels of deforestation in each region (9.6 M km2 in the Boreal zone vs. 10.2 M km2 in the tropics).

The most notable qualitative difference between regions relates to the emitted longwave flux changes, which are strongly negative in the Boreal region and essentially neutral in tropics for the coupled simulations. In the tropics, decreases in latent and sensible heat fluxes outweigh increases in shortwave reflectivity, requiring that the surface temperature and corresponding upward longwave fluxes increase to compensate. This may indicate that the decrease in latent and sensible heat flux in the tropics is dominated by a decrease in surface roughness, which reduces the efficiency of turbulent energy fluxes, rather than the albedo change that dominates in the Boreal forest.

3.4 Feedback Mechanisms

Lower temperatures in the FFICT scenario relative to the UCT scenario are associated with greater snow and ice extent (Figure 7), which contribute to the coupled increase in, reflected solar radiation (Figure 8) and represent a positive feedback on temperature reductions. The increase in reflected solar radiation in the coupled simulation is also due in part to an increase in incident solar radiation. Changes in water vapor and atmospheric dynamics combine to reduce cloud cover in many regions (Figure 7), particularly at high latitudes. This increase in insolation is partially reflected, but also provides more energy to drive latent, sensible, and long wave energy fluxes. The increase in sensible heat flux from the offline to coupled simulation is consistent with increased insolation, but the corresponding

decrease in latent heat also indicates a shift in Bowen ratio, probably due to lower surface temperatures and so lower vapor pressure deficit.

Indeed, reductions in latent heat flux and cooler air temperatures contribute to lower atmospheric water vapor, both in the tropics and at high Northern latitudes (Figure 9). Because the baseline level of atmospheric water vapor is quite low to begin with at high latitudes, this change leads to a significant change in the local greenhouse effect, defined as the difference between emitted surface longwave radiation and the top-of-atmosphere outward radiation flux. However, this effect is diminished in the tropics where the greenhouse effect of water vapor is more highly saturated. The spatial pattern of greenhouse effect changes is shown in Figure 10, which corresponds closely with the spatial pattern of temperature change shown in Figure 4. In the high latitudes, this cycle suggests a strong positive feedback effect – albedo and transpiration changes cool the air and reduce water vapor, which leads to lower downward longwave emission from the atmosphere. This, in turn, further cools the surface and reduces transpiration and water vapor. The decrease in emitted long wave and latent heat fluxes in the coupled simulation (Figure 6) is consistent with this mechanism. However, to definitively isolate the role of snow, ice, cloud, and water vapor feedbacks on the surface energy budget would require additional simulations targeting each mechanism individually.

Error! Reference source not found. shows changes in the planetary energy budget over the 21st century that result from greenhouse gas and albedo effects in both the UCT and FFICT scenario. Because the radiative forcing from anthropogenic GHGs is held fixed at

approximately 4.5 W/m^2 for each scenario, deviations in the greenhouse effect from this level are due to changes in atmospheric water vapor and temperature. In the UCT scenario, water vapor feedback effects increase the greenhouse effect from 4.5 W/m^2 to 5.6 W/m^2, while in the FFICT scenario, land-use change effects on water vapor reduce this to 4.1 W/m^2. Both scenarios exhibit positive albedo feedbacks that result from loss of snow of and ice over the 21st century, however these effects are reduced in the FFICT scenario (0.5 W/m^2) compared to the UCT scenario (1.2 W/m^2).

3.5 Radiative Forcing

Using the offline radiative transfer model to hold the 3-dimensional atmospheric conditions fixed at UCT scenario values while altering surface albedos according to the FFICT-offline scenario, we obtain a shift in top-of-atmosphere net downward shortwave flux of -0.96 W/m^2 for the period 2091-2100. Thus, the globally averaged forcing from land-use change in the FFICT scenario relative to UCT is on the same order of magnitude as forcing from anthropogenic GHGs in these scenarios.

4 Discussion

The results of this study indicate that under plausible scenarios, the biophysical climate effects of land-use change play an important role in determining the outcomes of climate policy at both global and regional scales. Thus policies that do not consider these effects may result in unintended consequences. In general, the climate outcomes of achieving

atmospheric GHG targets depend on the specific policy mechanisms employed insofar as those different mechanisms impact the pattern and scale of land-use change.

In the context of the CMIP5 simulations, these findings challenge a fundamental assumption underlying the "parallel process" (Moss et al., 2010) for generating alternative technological and socio-economic pathways for meeting the RCP targets, namely the assumption that there is a unique relationship between the trajectory of radiative forcing and subsequent climate change impacts as predicted by any given CMIP5 climate model. Furthermore, these results indicate that the RCP scenarios, which vary unsystematically in their levels and patterns of land-use change, may exhibit important differences in terms of regional and global climate outcomes that are not directly linked to the chosen GHG target. As a result, the transient climate sensitivity– i.e., the magnitude of temperature change in 2100 per unit of quantified forcing – exhibited by each CMIP5 model is likely to differ by scenario as well.

In addition to influencing the global mean temperature response, we show that land-use change can influence the spatial pattern or "fingerprint" of warming that is exhibited over time as derived from EOF analysis. This result has implications for the use of pattern scaling techniques for generating new climate change scenarios. See for example, (Mitchell, 2003). While it is possible to generate and scale separate response signals for GHG, aerosols, land-use change etc., the response signal for land-use change is highly dependent on geography and is likely to interact with GHG forcing. For example, the albedo response from Boreal deforestation depends on snow cover, which in turn is influenced by GHG-induced warming. The problem of geographic dependence has been addressed for aerosols

in the pattern-scaling literature by deriving separate response signals by region (Schlesinger et al., 2000).

As this work demonstrates, the forcing effect of land-use change is an important consideration for climate policy, both real and simulated. Land-use change is similar in some regards to sulfur aerosols, which are important despite their short atmospheric lives and geospatially heterogeneous effects on the Earth's energy balance. Depending on the specific objectives of individual policies, it may be appropriate to incorporate the forcing effect of albedo change into targets and accounting frameworks. If so, this work points to the inadequacy of globally averaged radiative forcing based solely on atmospheric constituents as the metric for doing so. As noted by others (Pielke et al., 2002), due to the geographically specific and spatially heterogeneous effect of land-use change on climate, globally averaged metrics belie the climate effects of land-use change on the regional scales where they matter most to humans. The global cooling effect of deforestation in these simulations is strongly concentrated in the high northern latitudes, whereas a radiatively equivalent reduction in GHG would be more evenly distributed across the globe, impacting society in different ways. Indeed, the cooling effect of Boreal deforestation is so concentrated that some regions experience net cooling over the 21st century in the FFICT scenario despite a global mean warming of 0.7° C.

Consistent with a growing body of evidence (Arora & Montenegro, 2011; Bala et al., 2007; Betts, 2000), this work demonstrates the significant regional cooling effect of Boreal deforestation, which results from strong albedo change coupled with a regional water vapor

greenhouse effect. The offline land model simulations demonstrate that reduced water vapor flux from the surface is only partially due to the first order effect of vegetation change. Atmospheric feedback processes further reduce this flux. While this experiment was not designed to separate different atmospheric processes from one another, a plausible explanation is that regional cooling driven by albedo change reduces the capacity of the atmosphere to retain water vapor and drives down latent heat fluxes, suggesting that albedo change can activate a high latitude water vapor feedback independently of changes in stomatal conductance.

The scale of surface energy and hydrological flux changes from tropical deforestation predicted by CESM is smaller than that indicated by eddy covariance studies (Randow et al., 2004). Despite this, we find significant temperature increases – on the order of 1 °C – in some regions of the tropics. Other modeling studies have found significant changes in precipitation resulting from tropical deforestation (Hasler, Werth, & Avissar, 2009; McGuffie et al., 1995; Nepstad, Stickler, Filho, & Merry, 2008). However, there is substantial disagreement among models on the magnitude and sometimes the sign of climatic effects from land-use change (Pitman et al., 2009). Thus, more work is needed to constrain model parameterizations with observational data before they can be used to make specific recommendations for programs such as REDD, which are likely to induce biophysical climate perturbations directly over large areas of the tropics and potentially indirectly outside the tropics via leakage mechanisms (Watson, 2000).

The integrated assessment model scenarios that that we examine assume that the biogeochemical climate effects of land-use change – that is, the associated CO_2 source and sink changes – are perfectly compensated for by reductions or increases in fossil carbon emissions. This assumption allows us to isolate the biophysical forcing and explore the implications of idealized policy scenarios. However, in practice it will be difficult to perfectly account for and trade the CO_2 fluxes from terrestrial sources – particularly those involving changes in soil carbon stocks – with those from fossil fuels. Many studies have examined the relative climate effects of biogeochemical and biophysical forcing from land-use change. Their results are mixed, but generally point to a stronger biogeochemical signal except for the case of Boreal deforestation where biophysical effects can dominate (Bala et al., 2007; Betts, 2000; Molen, Hurk, & Hazeleger, 2011). Regardless of which signal dominates, if the CO_2 flux from deforestation in the FFICT scenario were not totally compensated for through carbon trading, the apparent cooling signal from deforestation would be reduced.

In these simulations we do not account for non-CO_2 emissions from biomass burning, such as black carbon, organic carbon, and ozone precursors. These species could have significant climate effects on short time scales and may impact ecosystem function and human health directly. In addition, we treat all crops and grasses identically and do not prescribe special crop phenology or management practices. Thus we only capture the gross energy flux changes associated with conversion from forest ecosystems to non-forest ecosystems. A recent effort to incorporate crop-specific parameterizations into CESM (Levis et al., 2012) indicates that the high amplitude annual cycle in crop leaf area compared to grasses can

induce important seasonal effects on precipitation and surface energy fluxes. Future work on the land use effects of climate policy would benefit from using such parameterizations. Indeed, crop phenology has been identified as a major source of variance across model predictions of the climate effects of land-use change (Pitman et al., 2009).

5 Acknowledgments

This work was supported by the Director, Office of Science, Office of Biological and Environmental Research, Climate Change Research Division, of the U.S. Department of Energy under Contract No. DE-AC02-05CH11231. In addition, this research used resources of the National Energy Research Scientific Computing Center, which is supported by the Office of Science of the U.S. Department of Energy under Contract No. DE-AC02-05CH11231. The CESM project is supported by the National Science Foundation and the Office of Science (BER) of the U.S. Department of Energy.

6 References

Arora, V. K., & Montenegro, A. (2011). Small temperature benefits provided by realistic afforestation efforts. *Nature Geoscience*, *4*(8), 514–518.

Bala, G., Caldeira, K., Wickett, M., Phillips, T., Lobell, D., Delire, C., & Mirin, A. (2007). Combined climate and carbon-cycle effects of large-scale deforestation. *Proceedings of the National Academy of Sciences*, *104*(16), 6550.

Betts, R. (2000). Offset of the potential carbon sink from boreal forestation by decreases in surface albedo. *Nature*, *408*, 187–190.

Betts, R., Falloon, P., & Goldewijk, K. (2007). Biogeophysical effects of land use on climate: Model simulations of radiative forcing and large-scale temperature change. *Agricultural and forest meteorology*, *14*, 216–233.

Bitz, C. M., Shell, K. M., Gent, P. R., Bailey, D. A., Danabasoglu, G., Armour, K. C., Holland, M. M., et al. (2012). Climate Sensitivity of the Community Climate System Model, Version 4. *Journal of Climate*, *25*(9), 3053–3070. doi:10.1175/JCLI-D-11-00290.1

Bonan, G. (2008). Forests and Climate Change: Forcings, Feedbacks, and the Climate Benefits of Forests. *Science*, *320*(5882), 1444–1449. doi:10.1126/science.1155121

Bonan, G. B., Pollard, D., & Thompson, S. L. (1992). Effects of boreal forest vegetation on global climate. *Nature*, *359*, 716–718.

California Air Resources Board. (2009). *Proposed regulation to implement the low carbon fuel standard, Vol I, Staff Report*.

Conley, A. J., Lamarque, J. F., & Vitt, F. (2012). PORT, a CESM tool for the diagnosis of radiative forcing. *Geoscientific Model Development*.

FAO, UNDP, UNEP. (2008). *UN-REDD: UN Collaborative Programme on Reducing Emissions from Deforestation and Forest Degradation in Developing Countries (UN-REDD)*.

Feddema, J. J., Oleson, K. W., Bonan, G. B., Mearns, L. O., Buja, L. E., Meehl, G. A., & Washington, W. M. (2005). The importance of land-cover change in simulating future climates. *Science*, *310*(5754), 1674–1678. doi:10.1126/science.1118160

Findell, K. L., Shevliakova, E., Milly, P. C. D., & Stouffer, R. J. (2007). Modeled Impact of Anthropogenic Land Cover Change on Climate. *Journal of Climate*, *20*(14), 3621–3634. doi:10.1175/JCLI4185.1

Foley, J., DeFries, R., Asner, G., & Barford, C. (2005). Global consequences of land use. *Science*, *309*, 570–574.

Gedney, N., & Valdes, P. (2000). The effect of Amazonian deforestation on the northern hemisphere circulation and climate. *Geophysical Research Letters*, *27*(19), 3053–3056.

Gent, P. R., Danabasoglu, G., Donner, L. J., Holland, M. M., Hunke, E. C., Jayne, S. R., Lawrence, D. M., et al. (2011). The Community Climate System Model Version 4. *Journal of Climate*, *24*(19), 4973–4991. doi:10.1175/2011JCLI4083.1

Hasler, N., Werth, D., & Avissar, R. (2009). Effects of tropical deforestation on global hydroclimate: a multimodel ensemble analysis. *Journal of Climate*, *22*(5), 1124–1141.

Hurtt, G. C., Chini, L.P., Frolking, S., Betts, R. A., Feddema, J., Fischer, G., Fisk, J. P., et al. (2011). Harmonization of land-use scenarios for the period 1500–2100: 600 years of global gridded annual land-use transitions, wood harvest, and resulting secondary lands. *Climatic change*, *109*(1-2), 117–161. doi:10.1007/s10584-011-0153-2

Hurtt, G., Frolking, S., Fearon, M., Moore, B., Shevliakova, E., Malyshev, S., Pacala, S., et al. (2006). The underpinnings of land-use history: Three centuries of global gridded land-use transitions, wood-harvest activity, and resulting secondary lands. *Global Change Biology*, *12*(7), 1208–1229.

Kim, H. S., Edmonds, J., Lurz, J., Smith, S. J., & Wise, M. (2006). The objECTS Framework for integrated Assessment: Hybrid Modeling of Transportation. *The Energy Journal*, *Hybrid Modeling*(Special Issue #2), 63–92.

Kvalevåg, M. M., Myhre, G., Bonan, G., & Levis, S. (2009). Anthropogenic land cover changes in a GCM with surface albedo changes based on MODIS data. (P. A. Dirmeyer, D. Niyogi, N. de Noblet-Ducoudré, R. E. Dickinson, & P. K. Snyder, Eds.)*International Journal of Climatology*, *30*(13), 2105–2117. doi:10.1002/joc.2012

Lamarque, J. F., Kyle, G. P., Meinshausen, M., Riahi, K., Smith, S. J., van Vuuren, D. P., Conley, A. J., et al. (2011). Global and regional evolution of short-lived radiatively-active gases and aerosols in the Representative Concentration Pathways. *Climatic change*, *109*, 1–22.

Lawrence, D. M., Oleson, K. W., Flanner, M. G., Fletcher, C. G., Lawrence, P. J., Levis, S., Swenson, S. C., et al. (2012a). The CCSM4 Land Simulation, 1850–2005: Assessment of Surface Climate and New Capabilities. *Journal of Climate*, *25*(7), 2240–2260. doi:10.1175/JCLI-D-11-00103.1

Lawrence, P. J., & Chase, T. N. (2010). Investigating the climate impacts of global land cover change in the community climate system model. (P. A. Dirmeyer, D. Niyogi, N. de Noblet-Ducoudré, R. E. Dickinson, & P. K. Snyder, Eds.)*International Journal of Climatology*, *30*(13), 2066–2087. doi:10.1002/joc.2061

Lawrence, P. J., Feddema, J. J., Bonan, G. B., Meehl, G. A., O'Neill, B. C., Oleson, K. W., Levis, S., et al. (2012b). Simulating the Biogeochemical and Biogeophysical Impacts of Transient Land Cover Change and Wood Harvest in the Community Climate System Model (CCSM4) from 1850 to 2100. *Journal of Climate*. doi:10.1175/JCLI-D-11-00256.1

Levis, S., Bonan, G. B., Kluzek, E., Thornton, P. E., Jones, A., Sacks, W. J., & Kucharik, C. J. (2012). Interactive crop management in the Community Earth System Model (CESM1): Seasonal influences on land-atmosphere fluxes. *J. Climate*. doi:doi: 10.1175/JCLI-D-11-00446.1

Livezey, R., & Chen, W. (1983). Statistical Field Significance and its Determination by Monte Carlo Techniques. *Monthly Weather Review*, *111*, 46–59.

Marland, G., Pielke, R. A., Sr, Apps, M., Avissar, R., Betts, R. A., Davis, K. J., Frumhoff, P. C., et al. (2003). The climatic impacts of land surface change and carbon management, and the implications for climate-change mitigation policy. *Climate Policy*, *3*(2), 149–157. doi:10.3763/cpol.2003.0318

McGuffie, K., Henderson-Sellers, A., Zhang, H., Durbidge, T., & Pitman, A. (1995). Global climate sensitivity to tropical deforestation. *Global and Planetary Change*, *10*, 97–128.

Meinshausen, M., Raper, S., & Wigley, T. (2011). Emulating coupled atmosphere-ocean and carbon cycle models with a simpler model, MAGICC6–Part 1: Model description and calibration. *Atmos. Chem. Phys*, *11*(4), 1417–1456.

Mitchell, T. D. (2003). Pattern scaling: an examination of the accuracy of the technique for describing future climates. *Climatic change*, *60*(3), 217–242.

Molen, M. K., Hurk, B. J. J. M., & Hazeleger, W. (2011). A dampened land use change climate response towards the tropics. *Climate Dynamics*, *37*(9-10), 2035–2043. doi:10.1007/s00382-011-1018-0

Moss, R. H., Edmonds, J. A., Hibbard, K. A., Manning, M. R., Rose, S. K., van Vuuren, D. P., Carter, T. R., et al. (2010). The next generation of scenarios for climate change research and assessment. *Nature*, *463*(7282), 747–756. doi:10.1038/nature08823

Nepstad, D. C., Stickler, C. M., Filho, B. S., & Merry, F. (2008). Interactions among Amazon land use, forests and climate: prospects for a near-term forest tipping point. *Philosophical Transactions of the Royal Society B: Biological Sciences*, *363*(1498), 1737–1746. doi:10.1098/rstb.2007.0036

Pielke, R., Sr, Marland, G., Betts, R., Chase, T., Eastman, J., Niles, J., Niyogi, D., et al. (2002). The influence of land-use change and landscape dynamics on the climate system: relevance to climate-change policy beyond the radiative effect of greenhouse gases. *Philosophical Transactions of the Royal Society*, *360*, 1705–1719.

Pitman, A., de Noblet-Ducoudré, N., Cruz, F., Davin, E., Bonan, G., Brovkin, V., Claussen, M., et al. (2009). Uncertainties in climate responses to past land cover change: First results from the LUCID intercomparison study. *Geophysical Research Letters*, *36*(14), L14814.

Randow, Von, C., Manzi, A. O., Kruijt, B., de Oliveira, P. J., Zanchi, F. B., Silva, R. L., Hodnett, M. G., et al. (2004). Comparative measurements and seasonal variations in energy and carbon exchange over forest and pasture in South West Amazonia. *Theoretical and Applied Climatology*, *78*(1-3). doi:10.1007/s00704-004-0041-z

Santer, B., Wigley, T., Simmons, A., Kållberg, P., Kelly, G., Uppala, S., Ammann, C., et al. (2004). Identification of anthropogenic climate change using a second-generation reanalysis. *Journal of Geophysical Research*, *109*.

Schlesinger, M. E., Malyshev, S., Rozanov, E. V., Yang, F., Andronova, N. G., De Vries, B., Grübler, A., et al. (2000). Geographical Distributions of Temperature Change for Scenarios of Greenhouse Gas and Sulfur Dioxide Emissions. *Technological Forecasting and Social Change*, *65*(2), 167–193. doi:10.1016/S0040-1625(99)00114-6

Swann, A., Fung, I., Levis, S., Bonan, G., & Doney, S. (2010). Changes in Arctic vegetation amplify high-latitude warming through the greenhouse effect. *Proceedings of the National Academy of Sciences*, *107*(4).

Taylor, K. E., Stouffer, R. J., & Meehl, G. A. (2011). A Summary of the CMIP5 Experimental Design, 1–33.

Thomson, A. M., Calvin, K. V., Chini, L.P., Hurtt, G., Edmonds, J. A., Bond-Lamberty, B., Frolking, S., et al. (2010). Climate mitigation and the future of tropical landscapes. *Proceedings of the National Academy of Sciences*, *107*(46), 19633–19638.

Thomson, A. M., Calvin, K. V., Smith, S. J., Kyle, G. P., Volke, A., Patel, P., Delgado-Arias, S., et al. (2011). RCP4. 5: a pathway for stabilization of radiative forcing by 2100. *Climatic change*, *109*, 77–94.

Thornton, P. E., Lamarque, J. F., Rosenbloom, N. A., & Mahowald, N. M. (2007). Influence of carbon-nitrogen cycle coupling on land model response to CO2 fertilization and climate variability. *Global Biogeochemical Cycles*, *21*(4), 1–15.

U.S. Congress. (2012). *American Clean Energy and Security Act of 2009* (No. H.R. 2454).

USEPA. (2010). *Renewable Fuel Standard Program (RFS2) Regulatory Impact Analysis*.

van Vuuren, D. P., Edmonds, J., Kainuma, M., Riahi, K., Thomson, A., Hibbard, K., Hurtt, G. C., et al. (2011). The representative concentration pathways: an overview. *Climatic change*, *109*(1-2), 5–31. doi:10.1007/s10584-011-0148-z

Watson, R. T. (2000). Land use, land-use change, and forestry. *IPCC Special Report*.

Wise, M., Calvin, K., Thomson, A., Clarke, L., Bond-Lamberty, B., Sands, R., Smith, S. J., et al. (2009). Implications of Limiting CO2 Concentrations for Land Use and Energy. *Science*, *324*(5931), 1183–1186. doi:10.1126/science.1168475

7 Tables

Table 1: Mean planetary energy budget changes from the first simulation decade (2005-2014) to the last (2090-2099) (last decade minus first) for both the UCT and FFICT scenarios. The greenhouse effect designates a decrease in top-of-atmosphere longwave radiation relative to surface longwave radiation and the albedo effect refers to an increase in net absorbed shortwave radiation

	Greenhouse Effect	Albedo Effect
	W/m^2	W/m^2
UCT	5.6	1.2
FFICT	4.1	0.5

8 Figure Captions

Figure 1: Change in a) crop cover and b) forest cover from 2005 to 2100 for the FFICT scenario.

Figure 2: Global mean surface temperature anomaly relative to the first decade of each simulation (2005-2014) for RCP 4.5, the GCAM 4.5 UCT and GCAM 4.5 FFICT. Data are smoothed using 10-year averages taken every 5 years. Dashed lines indicate the 95% confidence interval around the RCP4.5 ensemble mean.

Figure 3: Spatial pattern of temperature change over the 21st century calculated using decadal differences (mean of the last simulation decade (2090-2099) minus the first (2005-2014)) for a) the UCT scenario and b) the FFICT scenario, as well as using EOF-based spatial fingerprint method for c) the UCT scenario and d) The FFICT scenario. The fingerprints have been scaled to fit within the range -1 to 1 °C.

Figure 4: Spatial pattern of mean surface temperature difference between the UCT and FFICT scenarios (FFICT minus UCT) for the final simulation decade (2090-2099), calculated a) annually, b) for the northern hemisphere summer: June, July and August (JJA), and c) for the northern hemisphere winter: December, January, and February (DJF). Stippling indicates those gridcells for which the FFICT value lies outside of the 95% confidence interval around the NCAR RCP4.5 ensemble mean.

Figure 5: Changes in the global land surface energy budget between the UCT and FFICT scenarios (FFICT minus UCT) for the final simulation decade (2090-2099) obtained from both offline land model simulations and fully coupled Earth system simulations that include atmospheric, ocean, and sea ice feedbacks. All fluxes are positive upward such that a

negative value for incident solar radiation designates an increase in insolation in the FFICT scenario relative to UCT. To the right of the dashed line are terms of the surface energy budget that are held fixed in the offline simulations.

Figure 6: Changes in the regional land surface energy budget for a) boreal ecosystems and b) tropical ecosystems between the UCT and FFICT scenarios (FFICT minus UCT) for the final simulation decade (2090-2099) obtained from both offline land model simulations and fully coupled Earth system simulations that include atmospheric, ocean, and sea ice feedbacks. All fluxes are positive upward such that a negative value for incident solar radiation designates an increase in insolation in the FFICT scenario relative to UCT. To the right of the dashed line are terms of the surface energy budget that are held fixed in the offline simulations. Note the change in scale relative to Figure. 5.

Figure 7: Fractional changes in a) snow cover, b) sea ice, and c) cloud cover between the coupled UCT and FFICT scenarios (FFICT minus UCT) for the final simulation decade (2090-2099).

Figure 8: Surface albedo changes between the UCT and FFICT scenarios (FFICT minus UCT) for the final simulation decade (2090-2099) based on a) offline land model simulations and b) fully coupled Earth system model simulations that account for atmospheric, ocean, and sea ice feedbacks.

Figure 9: Mean atmospheric water vapor content in the final simulation decade (2090-2099) by latitude and height (measured in pressure units) for a) the UCT scenario and b) the difference between UCT and FFICT scenarios (FFICT minus UCT).

Figure 10: Spatial pattern of difference in the greenhouse effect during the final simulation decade (2090-2099) between the UCT and FFICT scenarios (FFICT minus UCT).

Table 1: Mean planetary energy budget changes from the first simulation decade (2005-2014) to the last (2090-2099) (last decade minus first) for both the UCT and FFICT scenarios. The greenhouse effect designates a decrease in top-of-atmosphere longwave radiation relative to surface longwave radiation and the albedo effect refers to an increase in net absorbed shortwave radiation

9 Figures

Figure 1: Change in a) crop cover and b) forest cover from 2005 to 2100 for the FFICT scenario.

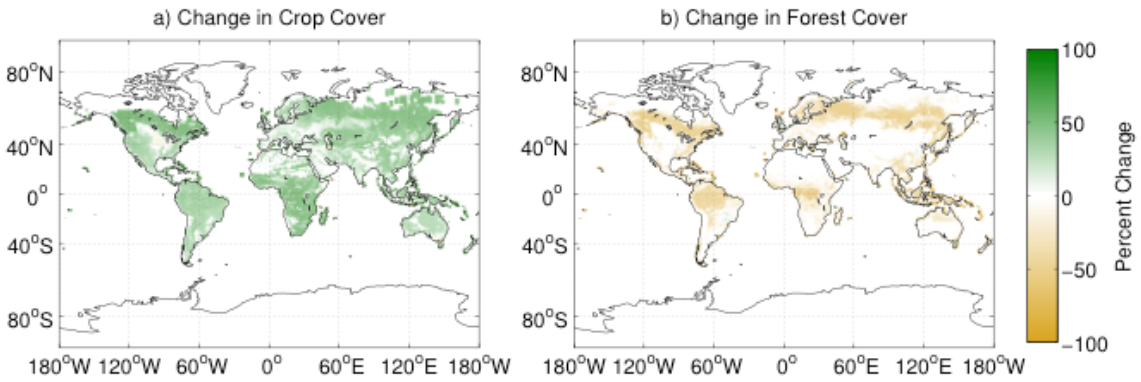

Figure 2: Global mean surface temperature anomaly relative to the first decade of each simulation (2005-2014) for RCP 4.5, the GCAM 4.5 UCT and GCAM 4.5 FFICT. Data are smoothed using 10-year averages taken every 5 years. Dashed lines indicate the 95% confidence interval around the RCP4.5 ensemble mean.

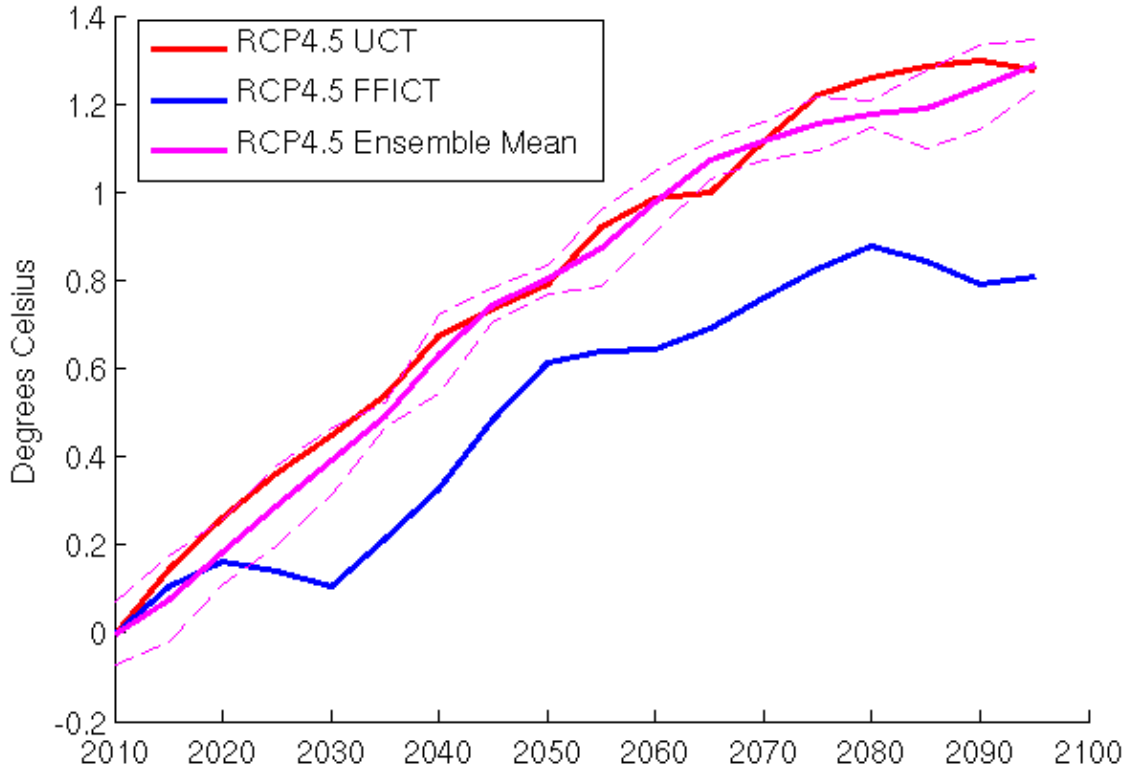

Figure 3: Spatial pattern of temperature change over the 21st century calculated using decadal differences (mean of the last simulation decade (2090-2099) minus the first (2005-2014)) for a) the UCT scenario and b) the FFICT scenario, as well as using EOF-based spatial fingerprint method for c) the UCT scenario and d) The FFICT scenario. The fingerprints have been scaled to fit within the range -1 to 1 °C.

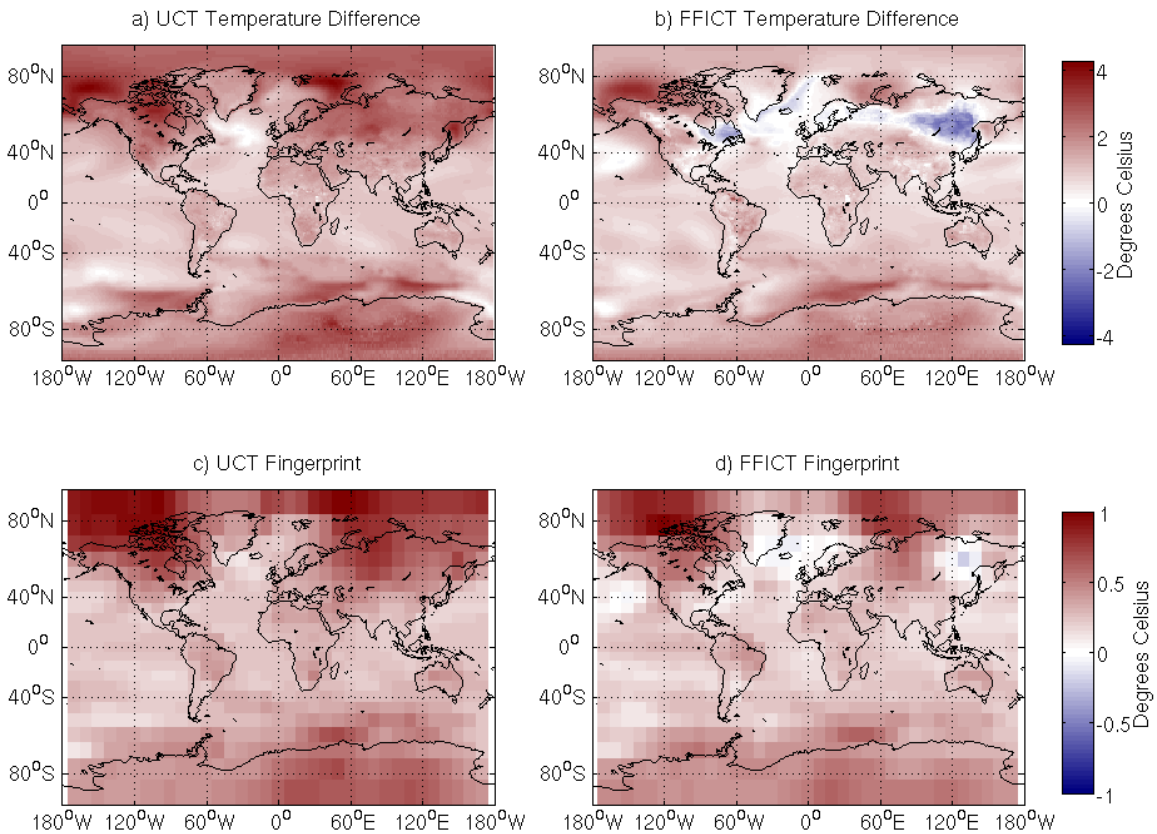

Figure 4: Spatial pattern of mean surface temperature difference between the UCT and FFICT scenarios (FFICT minus UCT) for the final simulation decade (2090-2099), calculated a) annually, b) for the northern hemisphere summer: June, July and August (JJA), and c) for the northern hemisphere winter: December, January, and February (DJF). Stippling indicates those gridcells for which the FFICT value lies outside of the 95% confidence interval around the NCAR RCP4.5 ensemble mean.

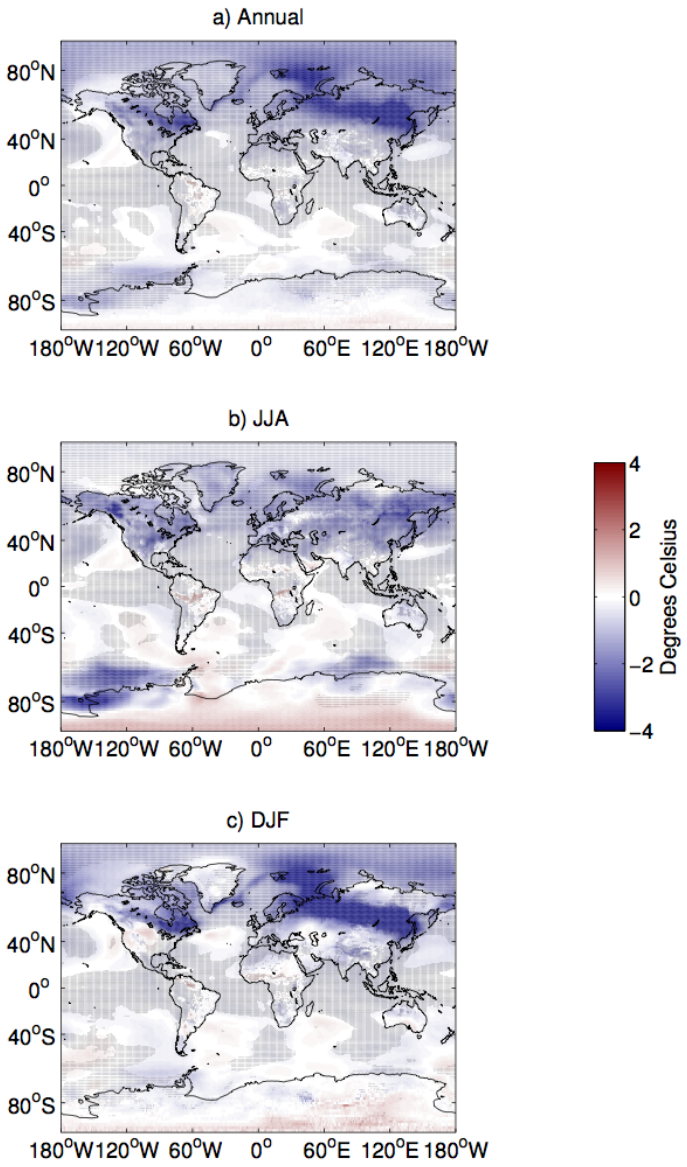

Figure 5: Changes in the global land surface energy budget between the UCT and FFICT scenarios (FFICT minus UCT) for the final simulation decade (2090-2099) obtained from both offline land model simulations and fully coupled Earth system simulations that include atmospheric, ocean, and sea ice feedbacks. All fluxes are positive upward such that a negative value for incident solar radiation designates an increase in insolation in the FFICT scenario relative to UCT. To the right of the dashed line are terms of the surface energy budget that are held fixed in the offline simulations.

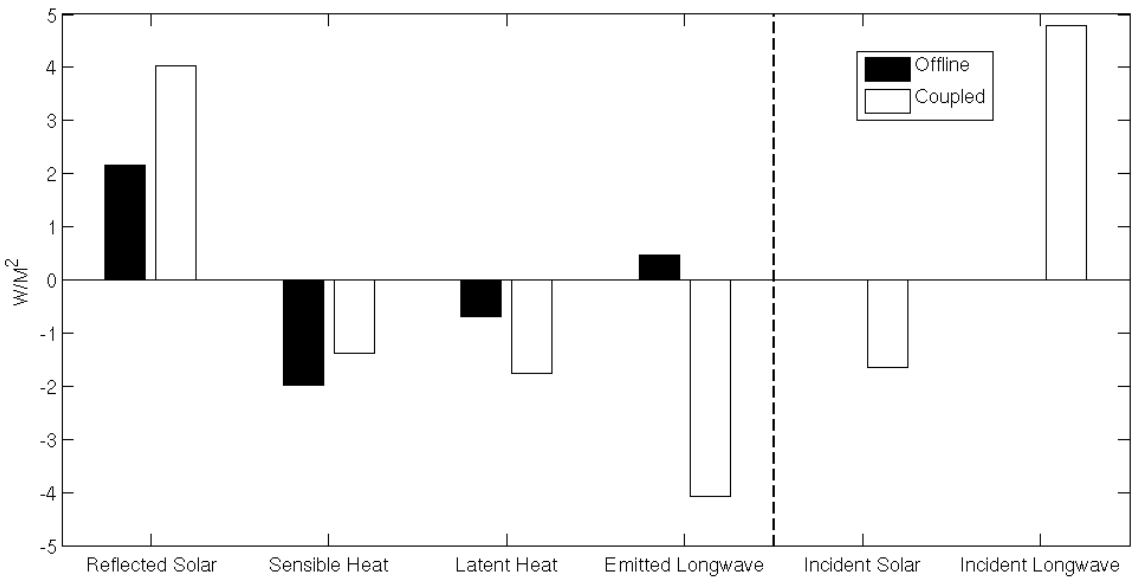

Figure 6: Changes in the regional land surface energy budget for a) boreal ecosystems and b) tropical ecosystems between the UCT and FFICT scenarios (FFICT minus UCT) for the final simulation decade (2090-2099) obtained from both offline land model simulations and fully coupled Earth system simulations that include atmospheric, ocean, and sea ice feedbacks. All fluxes are positive upward such that a negative value for incident solar radiation designates an increase in insolation in the FFICT scenario relative to UCT. To the right of the dashed line are terms of the surface energy budget that are held fixed in the offline simulations. Note the change in scale relative to Figure. 5.

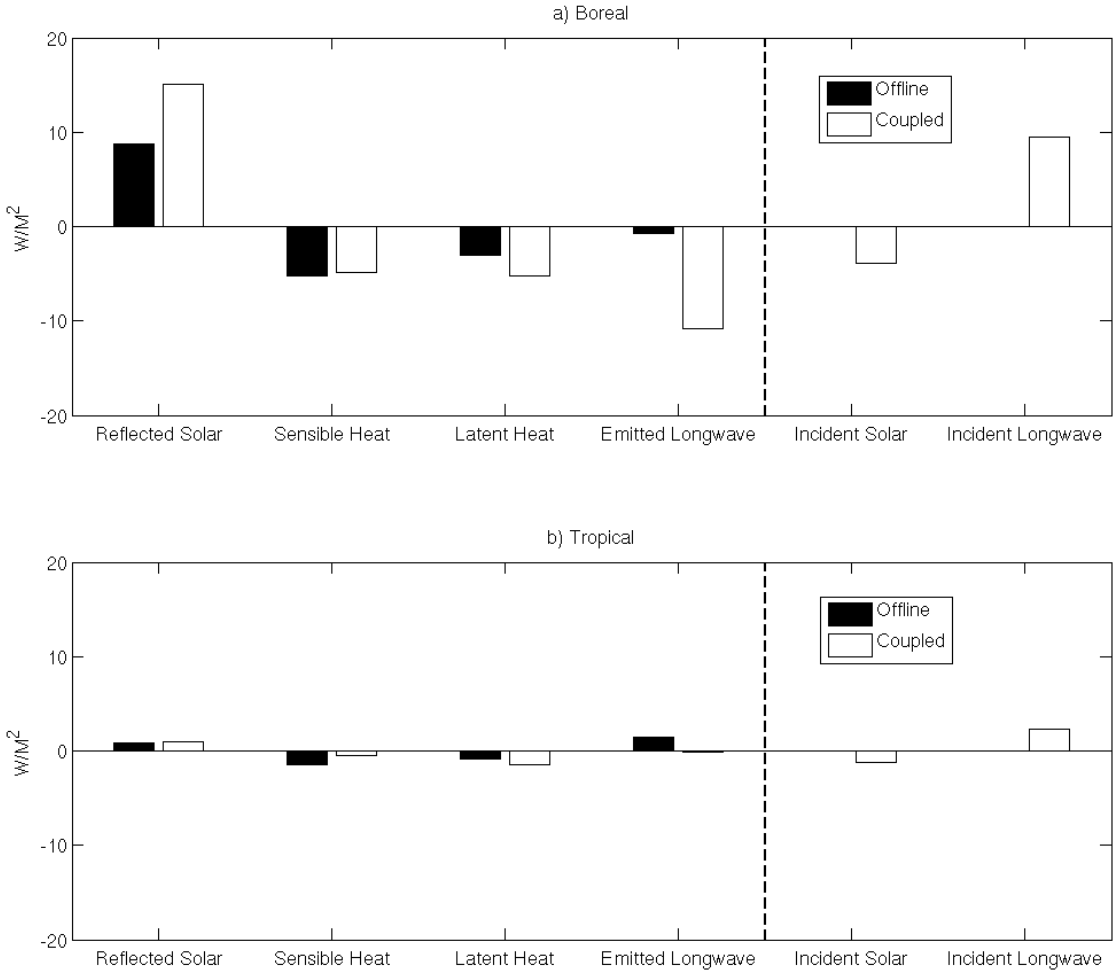

Figure 7: Fractional changes in a) snow cover, b) sea ice, and c) cloud cover between the coupled UCT and FFICT scenarios (FFICT minus UCT) for the final simulation decade (2090-2099).

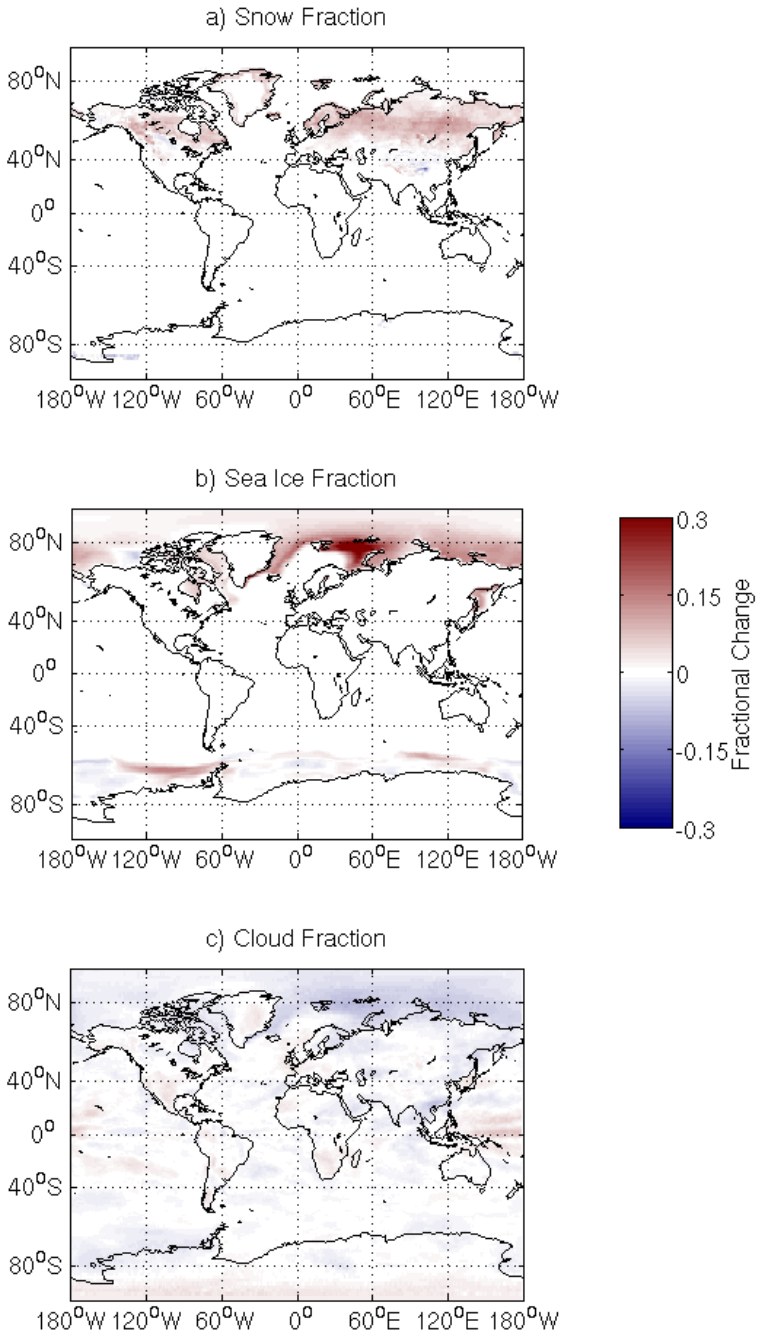

Figure 8: Surface albedo changes between the UCT and FFICT scenarios (FFICT minus UCT) for the final simulation decade (2090-2099) based on a) offline land model simulations and b) fully coupled Earth system model simulations that account for atmospheric, ocean, and sea ice feedbacks.

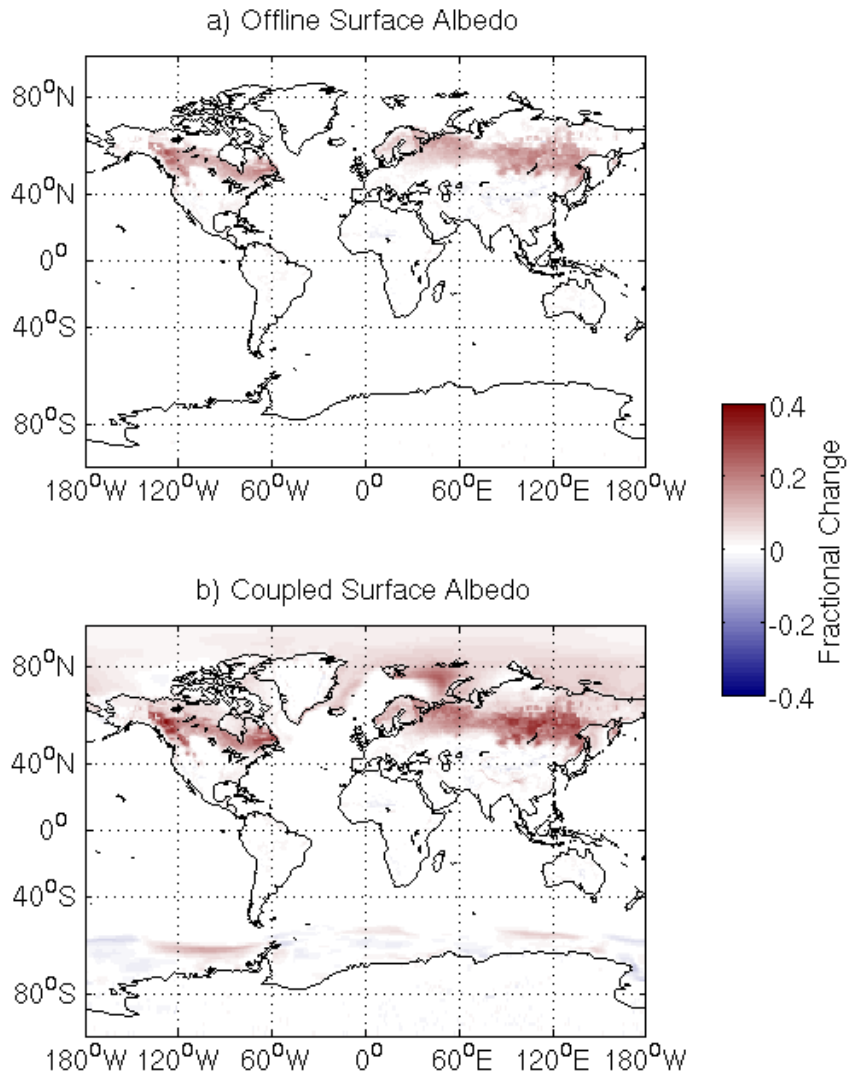

Figure 9: Mean atmospheric water vapor content in the final simulation decade (2090-2099) by latitude and height (measured in pressure units) for a) the UCT scenario and b) the difference between UCT and FFICT scenarios (FFICT minus UCT)

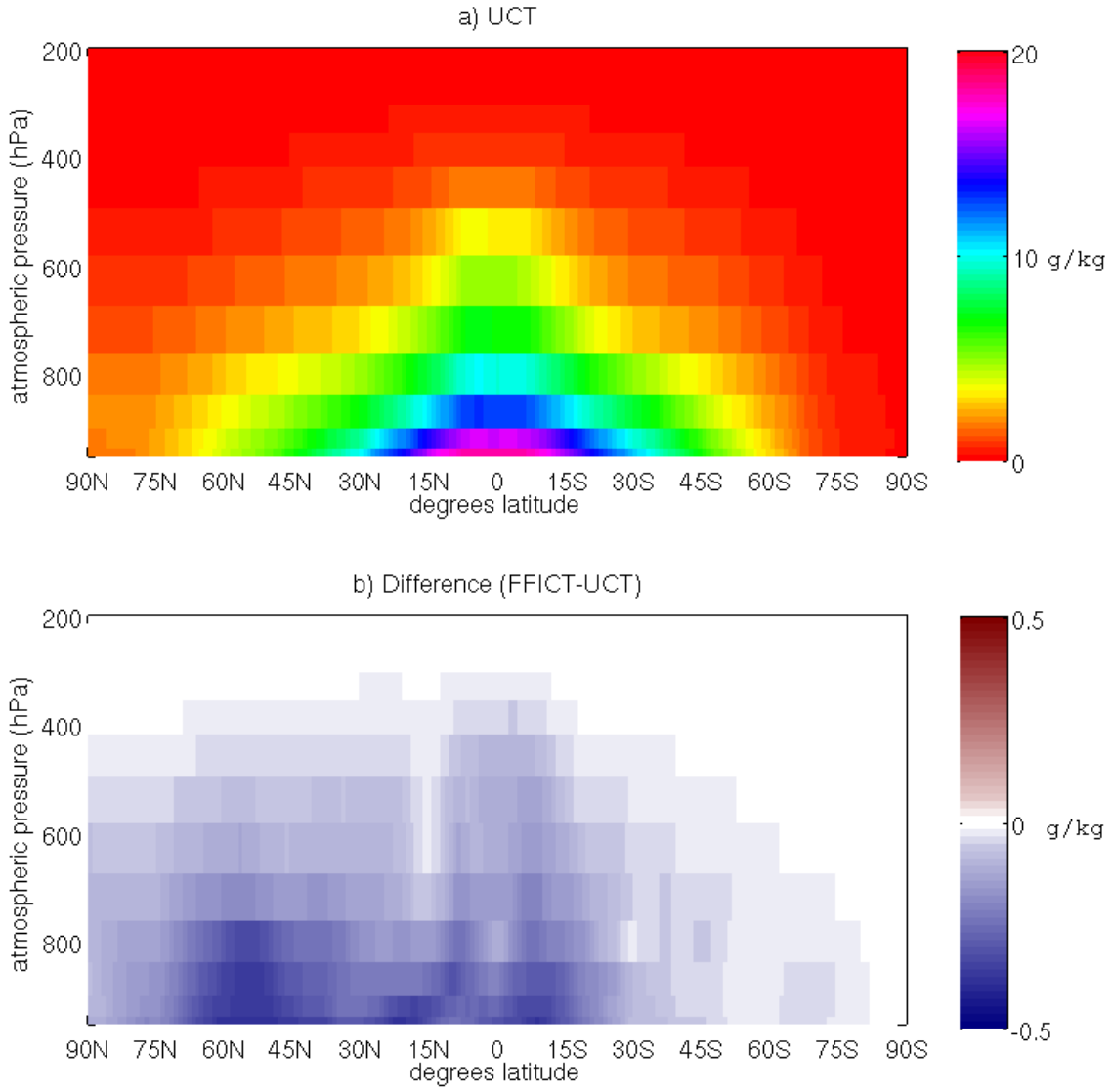

Figure 10: Spatial pattern of difference in the greenhouse effect during the final simulation decade (2090-2099) between the UCT and FFICT scenarios (FFICT minus UCT).

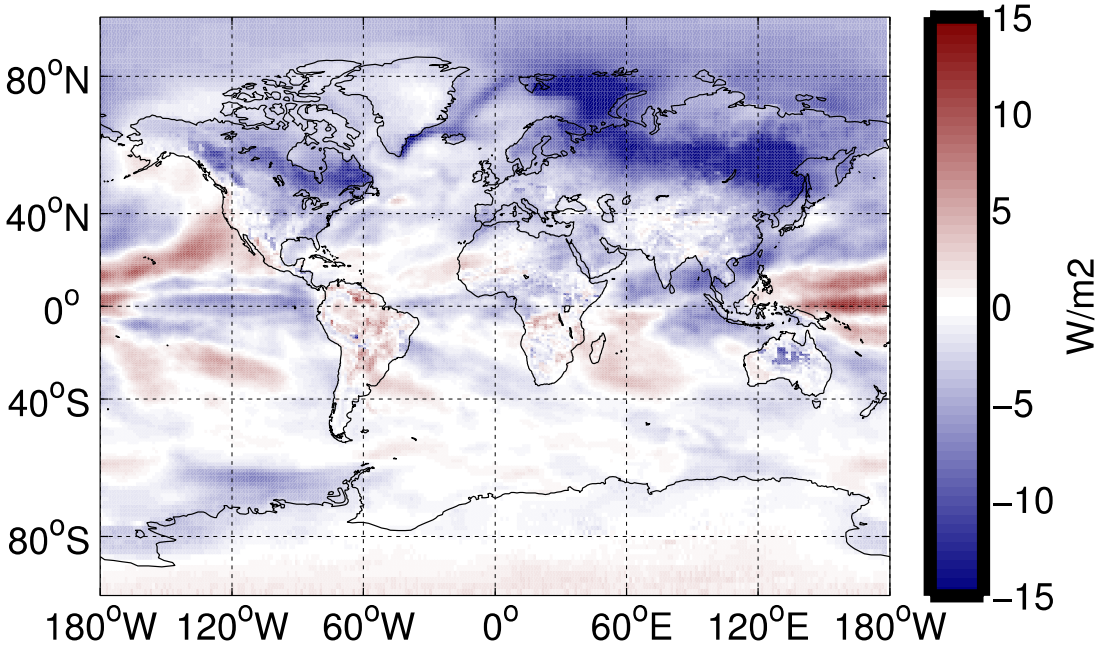

DISCLAIMER

This document was prepared as an account of work sponsored by the United States Government. While this document is believed to contain correct information, neither the United States Government nor any agency thereof, nor The Regents of the University of California, nor any of their employees, makes any warranty, express or implied, or assumes any legal responsibility for the accuracy, completeness, or usefulness of any information, apparatus, product, or process disclosed, or represents that its use would not infringe privately owned rights. Reference herein to any specific commercial product, process, or service by its trade name, trademark, manufacturer, or otherwise, does not necessarily constitute or imply its endorsement, recommendation, or favoring by the United States Government or any agency thereof, or The Regents of the University of California. The views and opinions of authors expressed herein do not necessarily state or reflect those of the United States Government or any agency thereof or The Regents of the University of California.

Ernest Orlando Lawrence Berkeley National Laboratory is an equal opportunity employer.